Suppressing the Kibble-Zurek mechanism by a symmetry-violating bias

J. Rysti,[1] J.T. Mäkinen,[1,*] S. Autti,[1,2] T. Kamppinen,[1] G.E. Volovik,[1,3] and V.B. Eltsov[1]

[1]*Department of Applied Physics, Aalto University, POB 15100, FI-00076 AALTO, Finland*
[2]*Department of Physics, Lancaster University, Lancaster LA1 4YB, UK.*
[3]*L.D. Landau Institute for Theoretical Physics, Moscow, Russia*
(Dated: July 16, 2021)

The formation of topological defects in continuous phase transitions is driven by the Kibble-Zurek mechanism. Here we study the formation of single- and half-quantum vortices during transition to the polar phase of ^{3}He in the presence of a symmetry-breaking bias provided by the applied magnetic field. We find that vortex formation is suppressed exponentially when the length scale associated with the bias field becomes smaller than the Kibble-Zurek length. We thus demonstrate an experimentally feasible shortcut to adiabaticity – an important aspect for further understanding of phase transitions as well as for engineering applications such as quantum computers or simulators.

In continuous phase transitions, random local choice of the symmetry-breaking order parameter leads to the formation of topological defects, such as quantized vortices. Originally a speculation in high-energy physics and cosmology [1], this mechanism, known as the Kibble-Zurek mechanism (KZM),[2–6], is now a cornerstone of out-of-equilibrium condensed matter physics. KZM has been observed in a range of systems such as superfluids, superconductors, and Bose condensates [7, 8]. In the KZM scenario the transition takes place independently in various regions with the characteristic size depending on the transition rate. Each region inherits a random realization of the broken-symmetry feature of the new phase, such as the phase of the order parameter in a superfluid transition. When the expanding regions merge, topological defects, such as quantized vortices, are formed. The predicted power-law dependence of the defect density on the quench rate has been confirmed in superfluid helium [9, 10] as well as in other systems (see e.g. [7, 8, 11]).

In the theory of broken-symmetry phase transitions, a symmetry-violating bias field plays an important role, initiating the choice between the different degenerate states [12]. Bias can in particular be applied to non-adiabatic thermodynamic [1, 2] or quantum [5] phase transitions that result in the formation of topological defects via the KZM. It has been proposed that if the applied symmetry-breaking bias is sufficiently large, the adiabatic (defect-free) regime is restored [13]. The crossover from the Kibble-Zurek regime to the adiabatic regime occurs at the characteristic value of the bias defined by the quench rate. Such crossover has been analyzed theoretically in a quantum phase transition in the Ising chain [13, 14] and in its classical counterpart [15]. Generally speaking, the KZM is expected to be modified in the presence of external factors such as inhomogeneities [16], or a propagating front of the phase transition [17]. Applying a bias allows for the external control of the magnitude of the KZM directly. Controlled restoration of the adiabatic regime by a symmetry-breaking bias can be utilized in applications requiring delicate and fast control of engineered quantum systems [13, 18].

In this Letter we probe experimentally the use of an external bias for suppressing the formation of single quantum vortices (SQV) and half-quantum vortices (HQV)[9, 19, 20] produced by the KZM in the phase transition from normal ^{3}He to the superfluid polar phase [21]. We report three central observations: (i) For HQVs the threshold bias for the onset of suppression is set by matching the characteristic length of the applied symmetry-breaking field to the Kibble-Zurek length, set by the quench rate. (ii) Beyond the onset, the suppression takes over exponentially, with the onset threshold normalizing the bias field in the exponent. (iii) The creation of SQVs is similarly suppressed for increasing bias fields while the threshold value is different from that for HQVs.

The spectrum of topological defects in the polar phase, and the bias fields one can apply, are understood in terms of the order parameter of the polar phase

$$A_{j\beta} = \Delta_{\rm P}\hat{\mathbf{d}}_j\hat{\mathbf{m}}_\beta e^{i\Phi}\,. \tag{1}$$

Here $\Delta_{\rm P}$ is the maximum gap in the quasiparticle energy spectrum and Φ is the superfluid phase. The unit vector $\hat{\mathbf{d}}$ determines the direction of the easy plane of the magnetic anisotropy and $\hat{\mathbf{m}}$ that of the orbital anisotropy. The anisotropy originates from p-wave Cooper pairing with the orbital momentum and spin of a pair equal to one. In the p-wave superfluid, confinement modifies the resulting order parameter [21, 23–28]. The polar phase is stabilized within the confining nanomaterial, which consists of nearly parallel solid strands, and $\hat{\mathbf{m}}$ is pinned along the strand direction, Fig. 1(a). The direction of $\hat{\mathbf{d}}$ is set by the competition between the magnetic anisotropy energy $\chi(\hat{\mathbf{d}}\cdot\mathbf{H})^2/2$ in the magnetic field $\mathbf{H}$, and the spin-orbit interaction energy $g_{\rm so}(\hat{\mathbf{d}}\cdot\hat{\mathbf{m}})^2$, where χ is the magnetic susceptibility and $g_{\rm so}$ is the spin-orbit coupling.

In large magnetic fields $H^2 \gg H^2_{\rm so} = g_{\rm so}\chi^{-1}$, the $\hat{\mathbf{d}}$ vector is kept in the plane perpendicular to $\mathbf{H}$ and the spin-orbit interaction takes the form

$$F_{\rm so} = g_{\rm so}\sin^2\mu\sin^2\alpha\,, \tag{2}$$

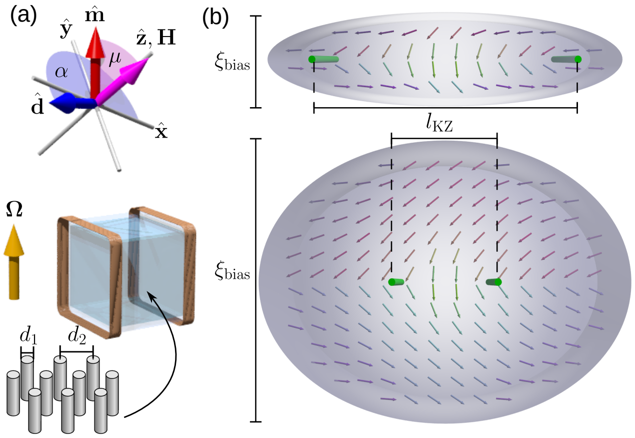

FIG. 1. Experimental principles. (a) The cubic $4\times4\times4$ mm^3 sample container is surrounded by NMR coils and filled with solid strands oriented along the vertical axis with the average diameter $d_1 = 9$ nm [22] and average separation $d_2 \approx 35$ nm. The space between the strands is filled with liquid ^{3}He. The magnetic field $\mathbf{H} \parallel \hat{\mathbf{z}}$ can be applied in any direction in the plane transverse to the NMR coil axes (angle μ is represented by the light red sector). The orbital anisotropy vector $\hat{\mathbf{m}}$ is pinned along the confining strands and the spin anisotropy vector $\hat{\mathbf{d}}$ is locked to the $\mathbf{xy}$ plane (light blue sector represents angle α) by $\mathbf{H}$. The sample can be rotated about the vertical axis with the angular velocity $\mathbf{\Omega}$ up to 3 rad s^{-1}. (b) The arrows represent the winding of $\hat{\mathbf{d}}$ by angle α (highlighted by the arrow colors) in the vicinity of two HQV cores (green cylinders). On a loop around a HQV core the $\hat{\mathbf{d}}$ vector rotates by π. For a large applied bias (Top) pairs of HQVs are connected by narrow $\hat{\mathbf{d}}$-solitons (highlighted with the background color) and the width of the soliton, giving the characteristic length scale of the applied bias field $\xi_{\rm bias}$, is much smaller than the KZ length, $\xi_{\rm bias} \ll l_{\rm KZ}$, resulting in suppression of the HQV formation in the phase transition to the superfluid phase. For a vanishing bias (Bottom) $\xi_{\rm bias} \gg l_{\rm KZ}$, the winding of the $\hat{\mathbf{d}}$-vector is nearly uniform, and formation of HQVs in the phase transition is not suppressed.

where μ is the angle between the magnetic field and the $\hat{\mathbf{m}}$ vector and α is the azimuthal angle of $\hat{\mathbf{d}}$ in the plane perpendicular to the magnetic field, see Fig. 1. For $\mu \neq 0$, the spin-orbit interaction in Eq. (2) lifts the degeneracy over α, playing the role of the symmetry-violating bias.

We first study the effect of applying a symmetry-breaking bias via the spin-orbit coupling. For a magnetic field oriented along the strands, $\mu = 0$, the spin-orbit bias is absent and the symmetry-breaking scheme (ignoring $SO(2)$ orbital rotations about $\hat{\mathbf{m}}$) is

$$G = U(1) \times SO(2) \to \Upsilon = Z_2 \,. \tag{3}$$

Here G describes the symmetries of normal ^{3}He, $U(1)$ is the symmetry under the phase transformation, and $SO(2)$ is the symmetry under rotation in spin space about the axis of the magnetic field. Υ denotes the symmetry of the polar phase order parameter, where Z_2 is the spin rotation by π (corresponding to the change $\hat{\mathbf{d}} \to -\hat{\mathbf{d}}$) accompanied by the phase change by π. Since the homotopy group $\pi_1(G/\Upsilon) = Z \times Z \times Z_2$, this symmetry-breaking scheme leads to three types of topological defects: SQVs in the superfluid phase (Φ-field), spin vortices in the orientation of the spin anisotropy vector (α-field), and HQVs, where both the superfluid phase Φ and the angle of the spin anisotropy vector α change by π.

When the spin-orbit interaction is turned on ($\mu \neq 0$), the $SO(2)$ symmetry in Eq.(3) is explicitly violated, and one obtains the following symmetry-breaking scheme:

$$\tilde{G} = U(1) \to \tilde{\Upsilon} = 1 \,. \tag{4}$$

Now the homotopy group is $\pi_1(\tilde{G}/\tilde{\Upsilon}) = Z$, which means that only SQVs remain stable, since they are not influenced by the spin-orbit interaction. Spin vortices and HQVs become termination lines of topological solitons [9, 19, 29–31], illustrated in Fig. 1(b). Assuming only HQVs are present, $\hat{\mathbf{d}}$-solitons connect pairs of HQVs of the opposite $\hat{\mathbf{d}}$-winding.

The presence of the solitons can be detected and their total volume in the sample measured using the nuclear magnetic resonance (NMR) techniques. The bulk of the sample forms the main peak in the continuous-wave NMR spectrum at the frequency $\omega_{\rm main}$, see Fig. S1 in Ref. [15]. The $\hat{\mathbf{d}}$-soliton provides a trapping potential for standing spin waves, seen as a satellite peak in the NMR spectrum at the frequency $\omega_{\rm sat}$ [9]. The relative sizes of the main peak and the satellite are determined by the volume occupied by the $\hat{\mathbf{d}}$-solitons in the sample. We note that the vortices created by the KZM are randomly oriented, but in our case the vortex density is low and thus the soliton volume connecting two HQVs is simply defined by the inter-vortex distance [15]. Measuring the initial density of KZ defects has traditionally been difficult due to the fast annihilation of non-equilibrium defects at temperatures close to the phase transition [3, 4, 10, 32]. In our experiments the confining strands pin vortices in place [9, 19, 30], providing the observer a frozen window to the out-of-equilibrium physics of the phase transition and a direct measurement of the KZ vortex density.

We calibrate the size of the satellite peak by preparing a state by a very slow cooldown through the critical temperature $T_{\rm c}$ at $H = 0$ while the sample is in rotation. This way we create HQVs with aerial density $n_{\rm v} = 4\Omega\kappa^{-1}$, where Ω is the angular velocity, $\kappa = h/(2m_3)$ is the quantum of circulation, h is the Planck constant, and m_3 is the ^{3}He atom mass. The calibration gives the relative satellite size $I_{\rm sat} = I_0\sqrt{\Omega}$, where $I_0 = 0.090$ s$^{1/2}$ rad$^{-1/2}$ [15]. The inter-vortex distance assuming a square lattice is

$$L = n_{\rm v}^{-1/2} = \frac{1}{2}\sqrt{\kappa}\frac{I_0}{I_{\rm sat}} \,. \tag{5}$$

We use this relation to calculate the HQV density and inter-vortex distance also for HQVs created purely by the

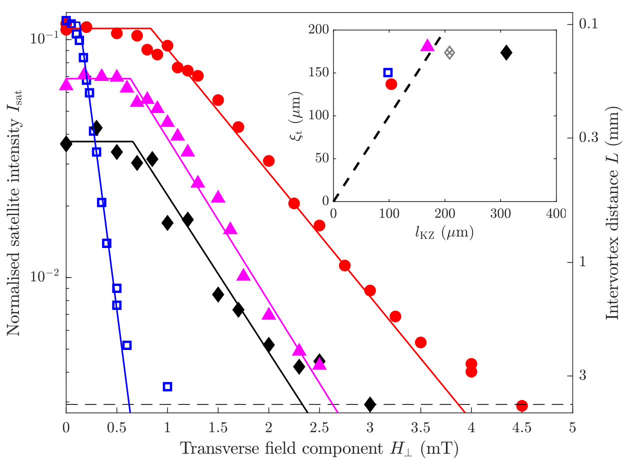

FIG. 2. Suppression of the HQV density created by the KZM as a function of the applied bias. Filled red circles, magenta triangles, and black diamonds correspond to quench rates of $\tau_Q \approx 3.8 \cdot 10^2$ s, $\tau_Q \approx 1.4 \cdot 10^3$ s, and $\tau_Q \approx 7.7 \cdot 10^3$ s, respectively, while applying a constant $H = 11$ mT magnetic field. The field is rotated to achieve different bias fields $H_\perp = H \sin\mu$. Open blue squares ($\tau_Q \approx 6.0 \cdot 10^2$ s) correspond to measurements with zero axial field component, $H_\perp = H$. Vortex density is constant for $H_\perp < H_{\perp t}$ and suppressed for higher bias fields. The suppression starts when the characteristic length scale of the bias field $\xi_{bias}(H_\perp)$ becomes smaller than the relevant Kibble-Zurek length. Solid lines correspond to theoretical model, see text for details. The dashed line shows where the intervotex distance becomes comparable with the container size. The inset shows the extracted threshold bias length ξ_t as a function of l_{KZ} with the same symbols. The dashed line is $\xi_t = l_{KZ}$. The patterned gray diamond is the same measurement as the black diamond, but with l_{KZ} on the horizontal axis replaced with an estimation of the transition front thickness l_F [15]. For other measurements, l_F lies beyond the right border of the plot.

KZM (i.e. for $\Omega = 0$). The combined effect of rotation and KZM is discussed in Ref. [15].

We control the spin-orbit bias by applying a fixed magnetic field of $H = 11$ mT with transverse component $H_\perp = H \sin\mu$ during the cooldown through T_c. We repeat cooldowns for different $H_\perp$ and different cooldown rates, Fig. 2. We observe a constant satellite size for small $H_\perp$ and its gradual suppression for larger values of $H_\perp$. We suggest that the threshold field $H_{\perp t}$ where the suppression of the formation of HQVs starts is determined by comparing the Kibble-Zurek length $l_{KZ} = a\xi_0(\tau_Q/\tau_0)^{1/4}$ with the characteristic length of the bias, ξ_{bias}, given by the thickness of the $\hat{\mathbf{d}}$ solitons. Here $a \sim 1$ fixes the exact length scale for the defect formation (in our measurements $a \approx 2.3$ [15]), the quench rate is $\tau_Q^{-1} = -\mathrm{d}(T/T_c)/\mathrm{d}t|_{T=T_c}$, T is temperature, t is time, ξ_0 is the superfluid coherence length at low temperature, $\tau_0 = \xi_0 v_F^{-1} \sim 1\,$ns is the order parameter relaxation time, v_F is the Fermi velocity, $\xi_{bias} \sim \xi_{so}/\sin\mu$, and $\xi_{so} = 17\ \mu$m is the dipole length [9].

Equating l_{KZ} with ξ_{bias} gives the following threshold bias for the suppression of HQV creation

$$H_{\perp t} = \frac{\xi_{so}}{l_{KZ}} H\,. \tag{6}$$

In the spirit of Ref. [13] we propose that the defect density $\propto I_{sat}^2$ decays exponentially after the transition field. In terms of the satellite intensity, this reads

$$I_{sat} = \begin{cases} I_{sat0} & \text{for } H_\perp < H_{\perp t} \\ I_{sat0}\exp\left(1 - H_\perp/H_{\perp t}\right) & \text{for } H_\perp \geq H_{\perp t}\,, \end{cases} \tag{7}$$

where I_{sat0} is the initial satellite intensity. We note that for this model $\int_0^\infty I_{sat}\mathrm{d}H_\perp = 2I_{sat0}H_{\perp t}$ and the numerical integral of the measured I_{sat} can be used to determine $H_{\perp t}$ without fitting.

Our experiments, Fig. 2, confirm the validity of the model (7). We use the zero-bias inter-vortex distance $L|_{H_\perp=0}$, Eq. (5), as the measured value of l_{KZ} [9, 32, 33]. We emphasize that the threshold field $H_{\perp t}$, which also normalizes the exponent, is determined by integration of the experimental data without a fitting procedure. The result agrees well with the conjecture $\xi_t \equiv \xi_{bias}(H_{\perp t}) = l_{KZ}$.

The result for the slowest quench rate deviates, however, from this dependence. In the presence of a thermal gradient, the phase transition proceeds via a propagating front, where the ordering of the low-temperature phase lags behind the temperature front where $T = T_c$ by distance l_F. The KZM operates in the band of width l_F and is modified in comparison to the homogeneous cooling scenario [17, 34, 35]. As τ_Q increases, l_F decreases and l_{KZ} increases. We suggest that the smaller of the two characteristic lengths, l_{KZ} and l_F, determines the threshold bias ξ_t. We estimate that in our measurement $l_F < l_{KZ}$ only for the slowest quench rate (black diamonds in Fig. 2) for which $l_F \sim 210\,\mu$m (gray patterned diamond in Fig. 2 inset), matching the observed value of ξ_t [15].

Alternatively we can apply a direct field bias with a weak magnetic field oriented perpendicular to $\hat{\mathbf{m}}$. The small magnetic field $H_\perp < H_{so}$ violates the symmetry under rotation about $\hat{\mathbf{m}}$, which leads to the formation of solitons, absent at zero magnetic field, with the soliton thickness now determined by the magnetic field directly, $\xi_{bias} = \xi_H = \xi_{so}H_{so}/H$. Equating ξ_{bias} with l_{KZ} yields a criterion for the threshold field similar to that in Eq. (6) but with H replaced by H_{so}. The expected decrease of the threshold field in this case is $H_{so}/H = \Omega_P/\omega_{main} \approx \sqrt{2(1-\omega_{sat}/\omega_{main})} \approx 0.17$ [9], where Ω_P is the polar phase Leggett frequency. It is confirmed experimentally by the blue squares in Fig. 2. Here the ratio of the threshold field relative to the red circles, which correspond to the spin-orbit bias with similar quench rate, is 0.16.

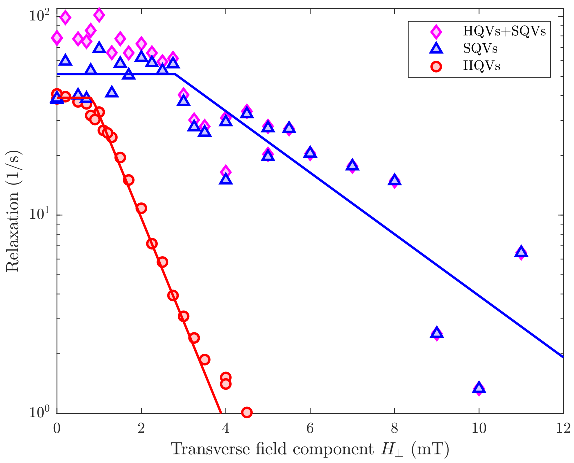

FIG. 3. Suppression of SQV density as a function of the applied bias. The measured magnon BEC relaxation rate (magenta diamonds) include contributions from HQVs and SQVs. The HQV contribution (red circles) is separated using linear NMR measurements of the satellite intensity and calibration from Ref. [30]. The remaining contribution to relaxation (blue triangles) we attribute to SQVs. The observed relaxation rates are compared to the suppression model (solid lines, Eq. (7)), and the red line corresponds to the same threshold as in Fig. 2. In these measurements the quench rate is $\tau_{\rm Q} \sim 4 \cdot 10^2$ s and the magnitude of the magnetic field is kept constant while its direction is varied. The largest transverse field value corresponds to $\mu = \pi/2$. Constant BEC relaxation rate not related to vortices has been subtracted.

Finally, we study the fate of SQVs under the symmetry-breaking bias created by tilting the magnetic field. Due to the absence of the topological solitons one would naïvely expect that the bias has no effect on the KZM for SQVs. Without the solitons, SQVs are not seen in continuous-wave NMR, but they were found to increase the relaxation rate of a magnon BEC [30, 36]. Independent measurements with SQVs created by rotation indicate that the BEC relaxation rate increases monotonically when the SQV density grows [30]. In our measurements we create both HQVs and SQVs by the KZM and subtract the effect of HQVs by using a calibration of the relaxation rate of the magnon BEC with respect to the satellite intensity, see Fig. 3b from Ref. [30]. The remaining contribution to the relaxation we attribute to SQVs. This contribution shows the characteristic dependence with a threshold and exponential suppression akin to Eq. (7), Fig. 3. A possible explanation for this behavior is that an applied bias influences the structure of the vortex core. For example in the superfluid B phase, the $SO(2)$ symmetry of the SQV core is spontaneously broken at low temperatures and the core transforms into a pair of tightly-bound half-quantum cores [37–39]. In the polar phase, the spin-orbit interaction and magnetic anisotropy may play the role of the symmetry-violating bias for the phase transitions inside the vortex core, but the detailed investigation remains a task for the future.

In conclusion, we report a crossover from the Kibble-Zurek regime of HQV creation to the adiabatic regime, where vortex formation is rapidly suppressed by a symmetry-violating bias. We thus demonstrate an experimentally feasible shortcut to adiabaticity, where the adiabatic regime can be reached without an infinitely slow transition rate. In our experiments the symmetry-violating bias is provided either by the spin-orbit interaction or directly by external magnetic field. The crossover to the adiabatic regime takes place when the characteristic length scale of the bias, given by the thickness of the topological solitons connecting neighboring HQVs, becomes smaller than the Kibble-Zurek length determined by the transition rate or the thickness of the transition front in the case of slow inhomogeneous cooling. Beyond the onset, the suppression of the KZM takes place exponentially. We also report similar suppression of SQV formation by the KZM, indicating that there may be a symmetry-breaking transition in the SQV core, sensitive to the symmetry-violating external bias.

The symmetry-breaking aspect of the bias field is essential for the suppression of the KZM, which otherwise is very robust. As an example [15], we show that adding an array of HQVs created by rotating the sample has no effect on the KZM even when the characteristic length scale of the added lattice becomes smaller than the Kibble-Zurek length. We also note that HQVs are composite defects, whose KZM formation is rarely studied experimentally, and that they are analogs of Alice strings [40–42]. The KZM formation of HQVs studied here may shed light to defect formation across phase transitions in theories considering such systems.

Our results can be generalized to the bias-induced restoration of adiabadicity in various phase transitions including quantum phase transitions, which could provide applications for technologies such as quantum simulators and computers [13, 18]. On a more speculative note, it is not excluded that the bias plays a role in the so-called collapse of the wave function in quantum mechanics. In principle, the latter can be seen as "phase transition" occurring in the continuous spectrum of an infinite system [43–45]. One of the many quantum states participating in a given quantum superposition is perhaps then selected by the infinitesimal bias unavoidably present in any experiment.

We thank V. V. Dmitriev for providing the NAFEN sample. This work has been supported by the European Research Council (ERC) under the European Union's Horizon 2020 research and innovation programme (Grant Agreement No. 694248) and by Academy of Finland project No. 332964. S.A. acknowledges support from the Jenny and Antti Wihuri Foundation via the Council of Finnish Foundations and T. K. acknowledges support from the Finnish Cultural Foundation. This research made use of the OtaNano – Low Temperature Laboratory infrastructure of Aalto University, that is part of the European Microkelvin Platform (European Union's Horizon 2020 Grant No. 824109).

J. R. and J. T. M. contributed equally to this work.

---

* jere.makinen@aalto.fi

[1] T. W. B. Kibble, J. Phys. A: Math. Gen. **9**, 1387 (1976).
[2] W. H. Zurek, Nature **317**, 505 (1985).
[3] V. M. H. Ruutu, V. B. Eltsov, A. J. Gill, W. B. Kibble, M. Krusius, Y. G. Makhlin, B. Placais, G. E. Volovik, and W. Xu, Nature **382**, 334 (1996).
[4] C. Bauerle, Y. M. Bunkov, S. N. Fisher, H. Godfrin, and G. R. Pickett, Nature **382**, 332 (1996).
[5] J. Dziarmaga, Physical Review Letters **95**, 245701 (2005).
[6] M. Prüfer, P. Kunkel, H. Strobel, S. Lannig, D. Linnemann, C.-M. Schmied, J. Berges, T. Gasenzer, and M. Oberthaler, Nature **563**, 217 (2018).
[7] A. Polkovnikov, K. Sengupta, A. Silva, and M. Vengalattore, Rev. Mod. Phys. **83**, 863 (2011).
[8] A. Del Campo and W. Zurek, International Journal of Modern Physics A **29** (2014).
[9] S. Autti, V. V. Dmitriev, J. T. Mäkinen, A. A. Soldatov, G. E. Volovik, A. N. Yudin, V. V. Zavjalov, and V. B. Eltsov, Phys. Rev. Lett. **117**, 255301 (2016).
[10] Y. M. Bunkov, A. I. Golov, V. S. L'vov, A. Pomyalov, and I. Procaccia, Phys. Rev. B **90**, 024508 (2014).
[11] J. Beugnon and N. Navon, Journal of Physics B: Atomic, Molecular and Optical Physics **50**, 022002 (2017).
[12] Y. G. Sinai, *Theory of Phase Transitions. Rigorous Results* (Pergamon Press, New York, 1982).
[13] M. M. Rams, J. Dziarmaga, and W. H. Zurek, Phys. Rev. Lett. **123**, 130603 (2019).
[14] B. Yan, V. Y. Chernyak, W. H. Zurek, and N. A. Sinitsyn, Phys. Rev. Lett. **126**, 070602 (2021).
[15] See the supplementary material at [*URL will be inserted by publisher*] for details.
[16] A. Del Campo, T. Kibble, and W. Zurek, Journal of Physics Condensed Matter **25** (2013).
[17] T. W. B. Kibble and G. E. Volovik, Journal of Experimental and Theoretical Physics Letters **65**, 102 (1997).
[18] A. del Campo and K. Kim, New Journal of Physics **21**, 050201 (2019).
[19] J. T. Mäkinen, V. V. Dmitriev, J. Nissinen, J. Rysti, G. E. Volovik, A. N. Yudin, K. Zhang, and V. B. Eltsov, Nature Communications **10** (2019).
[20] R. C. Regan, J. J. Wiman, and J. A. Sauls, (2021), arXiv:2105.01257 [cond-mat.supr-con].
[21] V. V. Dmitriev, A. A. Senin, A. A. Soldatov, and A. N. Yudin, Phys. Rev. Lett. **115**, 165304 (2015).
[22] V. E. Asadchikov, R. S. Askhadullin, V. V. Volkov, V. V. Dmitriev, N. K. Kitaeva, P. N. Martynov, A. A. Osipov, A. A. Senin, A. A. Soldatov, D. I. Chekrygina, and A. N. Yudin, JETP Lett. **101**, 556 (2015).
[23] L. V. Levitin, R. G. Bennett, A. Casey, B. Cowan, J. Saunders, D. Drung, T. Schurig, and J. M. Parpia, Science **340**, 841 (2013).
[24] J. I. A. Li, A. M. Zimmerman, J. Pollanen, C. A. Collett, and W. P. Halperin, Phys. Rev. Lett. **114**, 105302 (2015).
[25] J. I. A. Li, J. Pollanen, A. M. Zimmerman, C. A. Collett, W. J. Gannon, and W. P. Halperin, Nature Communications **10** (2019).
[26] L. V. Levitin, B. Yager, L. Sumner, B. Cowan, A. J. Casey, J. Saunders, N. Zhelev, R. G. Bennett, and J. M. Parpia, Phys. Rev. Lett. **122**, 085301 (2019).
[27] A. J. Shook, V. Vadakkumbatt, P. Senarath Yapa, C. Doolin, R. Boyack, P. H. Kim, G. G. Popowich, F. Souris, H. Christani, J. Maciejko, and J. P. Davis, Phys. Rev. Lett. **124**, 015301 (2020).
[28] V. V. Dmitriev, M. S. Kutuzov, A. A. Soldatov, and A. N. Yudin, (2020), arXiv:2012.06302 [cond-mat.other].
[29] V. P. Mineyev and G. E. Volovik, Physical Review B **18**, 3197 (1978).
[30] S. Autti, J. T. Mäkinen, J. Rysti, G. E. Volovik, V. V. Zavjalov, and V. B. Eltsov, Phys. Rev. Research **2**, 033013 (2020).
[31] G. E. Volovik, J. Rysti, J. T. Mäkinen, and V. B. Eltsov, Journal of Low Temperature Physics **196**, 82 (2019).
[32] V. B. Eltsov, M. Krusius, and G. E. Volovik, *Progr. in Low Temp. Phys.*, Vol. XV, p. 1-137 (Elsevier, 2005).
[33] C. Bäuerle, Y. M. Bunkov, S. N. Fisher, H. Godfrin, and G. R. Pickett, J Low Temp. Phys. **110**, 13 (1998).
[34] N. B. Kopnin and E. V. Thuneberg, Phys. Rev. Lett. **83**, 116 (1999).
[35] C.-R. Yi, S. Liu, R.-H. Jiao, J.-Y. Zhang, Y.-S. Zhang, and S. Chen, Phys. Rev. Lett. **125**, 260603 (2020).
[36] S. Autti, V. V. Dmitriev, J. T. Mäkinen, J. Rysti, A. A. Soldatov, G. E. Volovik, A. N. Yudin, and V. B. Eltsov, Phys. Rev. Lett. **121**, 025303 (2018).
[37] E. V. Thuneberg, Physical Review Letters **56**, 359 (1986).
[38] M. M. Salomaa and G. E. Volovik, Physical Review Letters **56**, 363 (1986).
[39] M. M. Salomaa and G. E. Volovik, Rev. Mod. Phys. **59**, 533 (1987).
[40] Y. Fujimoto and M. Nitta, Phys. Rev. D **103**, 054002 (2021).
[41] C. Chatterjee and M. Nitta, J. High Energ. Phys. **2017**, 46 (2017).
[42] T. Okada and Y. Sakatani, J. High Energ. Phys. **2015**, 131 (2015).
[43] M. Grady, arXiv:hep-th/9409049 (1994).
[44] G. Volovik, Lecture Notes in Physics **718**, 31 (2007).
[45] H. Ziaeepour, arXiv:1305.4349 (2018).